

# Mechanism and control of the structural evolution of a polymer solar cell from a bulk heterojunction to a thermally unstable hierarchical structure†

Cite this: *Nanoscale*, 2013, 5, 7629

Charn-Ying Chen,<sup>‡a</sup> Cheng-Si Tsao,<sup>‡\*a</sup> Yu-Ching Huang,<sup>‡a</sup> Hung-Wei Liu,<sup>‡b</sup> Wen-Yen Chiu,<sup>bc</sup> Chih-Min Chuang,<sup>a</sup> U-Ser Jeng,<sup>d</sup> Chun-Jen Su,<sup>d</sup> Wei-Ru Wu,<sup>d</sup> Wei-Fang Su<sup>e</sup> and Leeyih Wang<sup>\*bf</sup>

We simultaneously employed grazing incidence small-angle and wide-angle X-ray scattering (GISAXS and GIWAXS) techniques to quantitatively study the structural evolution and kinetic behavior of poly(3-hexylthiophene) (P3HT) crystallization, [6,6]-phenyl-C<sub>61</sub>-butyric acid methyl ester (PCBM) aggregation and amorphous P3HT/PCBM domains from a bulk heterojunction (BHJ) to a thermally unstable structure. The independent phase separation regimes on the nanoscale (~10 nm), mesoscale (~100 nm) and macroscale (~μm) are revealed for the first time. Bis-PCBM molecules as inhibitors incorporated into the P3HT/PCBM blend films were adopted as a case study of a control strategy for improving the thermal stability of P3HT/PCBM solar cell. The detailed information on the formation, growth, transformation and mutual interaction between different phases during the hierarchical structural evolution of P3HT/PCBM:xbis-PCBM (x = 8–100%) blend films are presented herein. This systematic study proposes the mechanisms of thermal instability for a polymer/fullerene-based solar cell. We demonstrate a new fundamental concept that the structural evolution and thermal stability of mesoscale amorphous P3HT/PCBM domains during heating are the origin of controlling thermal instability rather than those of nanoscale thermally-stable BHJ structures. It leads to a low-cost and easy-fabrication control strategy for effectively tailoring the hierarchical morphology against thermal instability from molecular to macro scales. The optimum treatment achieving high thermal stability, control of mesoscale domains, can be effectively designed. It is independent of the original BHJ nanostructure design of a polymer/fullerene-based solar cell with high performance. It advances the general knowledge on the thermal instability directly arising from the nanoscale structure.

Received 19th February 2013

Accepted 22nd May 2013

DOI: 10.1039/c3nr00864a

[www.rsc.org/nanoscale](http://www.rsc.org/nanoscale)

## Introduction

Bulk heterojunction (BHJ) polymer solar cells demonstrate great potential for commercialization and wide applications because of the characteristics of low cost, light weight, mechanical flexibility and easy manufacture (printable, roll-to-roll and

solution-processed).<sup>1–5</sup> It was extensively reported that the power conversion efficiency (PCE) of conjugated polymer/fullerene-derivative solar cells critically depends on the three-dimensional (3D) phase-separated BHJ structure of the active layer tailored by thermal annealing,<sup>2,6</sup> solvent treatment<sup>7</sup> or the use of solvent additives.<sup>8–13</sup> This nanostructure (or film morphology), comprised of (1) self-organized (or ordered) polymer as the donor, (2) aggregated fullerene molecules as the acceptor and (3) amorphous polymer/fullerene domains, constructs a bi-continuous interpenetrating network for effective charge separation at the donor–acceptor interface and charge carrier transport to the respective electrodes.<sup>14–25</sup> However, such a phase-separated BHJ structure is not thermodynamically stable (*i.e.*, in a non-equilibrium state) and would kinetically degrade under long-term exposure at elevated temperatures, finally leading to the low PCE.<sup>3–5,14–17</sup> To date, thermal stability of polymer/fullerene solar cells is the bottleneck for future commercialization. There are few reports fundamentally investigating the thermal degradation<sup>5,26–28</sup> in contrast to the extensive research on the device performance of polymer solar

<sup>a</sup>Institute of Nuclear Energy Research, Longtan, Taoyuan 32546, Taiwan. E-mail: [cstsao@iner.gov.tw](mailto:cstsao@iner.gov.tw)

<sup>b</sup>Institute of Polymer Science and Engineering, National Taiwan University, Taipei 10617, Taiwan. E-mail: [leewang@ntu.edu.tw](mailto:leewang@ntu.edu.tw)

<sup>c</sup>Department of Chemical Engineering, National Taiwan University, Taipei 10617, Taiwan

<sup>d</sup>National Synchrotron Radiation Research Center, Hsinchu 30077, Taiwan

<sup>e</sup>Department of Materials Science and Engineering, National Taiwan University, Taipei 10617, Taiwan

<sup>f</sup>Center for Condensed Matter Sciences, National Taiwan University, Taipei 10617, Taiwan

† Electronic supplementary information (ESI) available: P3HT and P3HT/PCBM GISAXS profiles and TEM images. See DOI: 10.1039/c3nr00864a

‡ These authors contributed equally.

cells. The current studies are also limited in microscopy observations, mainly reporting the macro- (or meso-) scale of phase segregation of the components under prolonged thermal annealing. This severe phase separation due to the thermal instability causes the large reduction in the donor-acceptor interface area and thus deteriorates the PCE.

Several strategies and approaches for suppressing the micro-sized phase segregation caused by the thermal degradation were developed with respect to the current knowledge from macroscopic observations. They are summarized as follows: (1) by reducing the regioregularity of the polymer chain or modifying the backbone of the polythiophenes, it can slow down the driving force of polymer crystallization and thus inhibit the formation of large-scale fullerene clusters, keeping the stable phase-separated BHJ structure during thermal annealing.<sup>29–31</sup> (2) The conjugated polymer with a high glass transition temperature as donor is utilized to freeze the fullerene clusters.<sup>32–34</sup> (3) The photocrosslinked or functionalized donor polymer can be used to form a polymer network for confining the large-scale motion of fullerene molecules during long-term heating.<sup>35,36</sup> (4) The addition of fullerene derivatives with different thiophene units as the surfactant (called a compatibilizer) into the polymer/fullerene blend films would improve the compatibility between the donor and acceptor phases to effectively suppress the coalescence at high temperatures.<sup>37–39</sup> (5) By incorporating the block copolymer additives, it can stabilize the structure of the BHJ film against destructive phase segregation.<sup>40,41</sup> (6) Some amorphous fullerene derivatives have been used to replace the commonly used [6,6]-phenyl-C<sub>61</sub>-butyric acid methyl ester (PCBM) as the acceptor. The blend polymer films with amorphous fullerene derivatives as an aggregation inhibitor retarding the phase segregation demonstrate the morphological stability against heating.<sup>42–44</sup>

There are general problems arising from the above approaches: (1) disturbing the crystallization of the conjugated polymer during fabrication annealing would lower the charge mobility, light-harvesting capability and even destroy the optimum morphology with the effective donor-acceptor interface. (2) Similarly, hindering the aggregation of the fullerene molecules using the aggregation inhibitor would destroy the nanoscale BHJ network and thus adversely influence the desired device performance (short-circuit current and PCE). (3) The initial treatment forming the optimum phase-separated nanomorphology may need to be redesigned due to the trade-off effect arising from the control strategy suppressing the micro-sized phase segregation (thermal instability). Simply speaking, there is a common understanding that the micro-sized phase segregation is caused by the coalescence of the nanoscale BHJ morphology (we will demonstrate that it is a misunderstanding). However, all current control strategies were based on this concept. To date, there is no mechanistic study. The characterization work reported on the thermal instability lacks the quantitative structural information at critical length scales, such as ~100 nm and down to 10 nm (~the diffusion length of an exciton), or even on a molecular scale. The mutual influence between polymer crystallization and fullerene aggregation on the multi-length scales during phase separation from a BHJ

structure to a thermally unstable structure is still under-investigation. To establish the rational strategy for improving thermal stability, it is critically important to study the mechanism of how the multi-length-scale structures of the donor and acceptor components evolve and mutually interact during the prolonged heating at high temperature. The thermal instability would be a usual degradation problem suffered in the practical fabrication step and in severe environments.

Grazing incidence small-angle and wide-angle X-ray scattering (GISAXS and GIWAXS) are powerful tools for investigating the hierarchical structure of bulk polymer/fullerene solar cells compared to the conventional microscopic and diffraction studies. GISAXS/GIWAXS provides a complementary insight to the microscopic observations due to the complexity of hierarchical structures. Recent review articles<sup>16,24,25</sup> have comprehensively summarized the investigations. The present work adopted the most-used polymer, poly(3-hexylthiophene) (P3HT), and PCBM as the donor and acceptor materials, respectively. We employed the simultaneous GISAXS and GIWAXS to study the P3HT/PCBM blend film from an as-cast state, then the BHJ state (regularly annealed at 150 °C for 5 min) to a thermally unstable structure (at 150 °C for 360 min). Quantitative data on the structural evolution and kinetic behavior of P3HT crystallization and PCBM aggregation at the nanoscale (~10 nm), mesoscale (10–100 nm) and macroscale (~μm) from a BHJ structure to a thermally unstable structure are revealed for the first time. The independent phase separation regimes on the multiple length scales are solved herein. The detailed information on the formation, growth, transformation and mutual interaction of different phases in the hierarchical structural evolution is presented herein. Moreover, the different amounts of bis-PCBM incorporated into the P3HT/PCBM blend films (the approach (6) previously mentioned) were adopted as a case study of how the thermal stability can be remarkably improved based on the proposed mechanism.<sup>44</sup> We employed GISAXS and GIWAXS to systematically and quantitatively investigate (1) how the bis-PCBM molecule manipulates the hierarchical structures comprised of the respective P3HT and PCBM components to effectively stabilize the film morphology (*i.e.*, PCBM/bis-PCBM blend as the acceptor); (2) how the different fullerene-derivatives (PCBM and bis-PCBM) as acceptor components interact with the polymer donor during the structural evolution of the various phase-separation stages (from the BHJ-forming stage up to the final unstable stage). This systematic study provides insight into the mechanism of thermal instability.

We demonstrate that the structural evolution and thermal stability of mesoscale amorphous P3HT/PCBM domains during heating is the origin of controlling thermal instability rather than those of nanoscale thermally-stable BHJ structures. The knowledge on mesoscale amorphous domains and their behavior from the current microscopic studies is limited. The thermal mechanism revealed here can provide a new fundamental concept as a breakthrough for a low-cost and easy-fabrication control strategy for effectively tailoring hierarchical morphology against thermal instability from molecular to macro scales. The rational design achieving high thermal

stability (effective control of the mesoscale domain) can additionally be an easy procedure with diverse routes, which is favorable for fabrication. It does not influence the original optimum BHJ nanostructure of a polymer/fullerene-based solar cell. This result could be extended to applications of morphological control of the thermal instability of general polymer/fullerene-based solar cells.

## Experimental details

PCBM (>99%) and bis-PCBM (>99.5%) were purchased from Nano-C and used as received. Regioregular P3HT ( $M_n = 4300 \text{ g mol}^{-1}$ , PDI = 1.3) was prepared using the Grignard metathesis method. The regioregularity was determined by  $^1\text{H}$  NMR to be greater than 95%. P3HT/PCBM BHJ blend films for the GISAXS/GIWAXS experiment were fabricated on a Si substrate by spin-coating. The films were then annealed at  $150^\circ\text{C}$  for either 5, 120 or 360 min, under an inert atmosphere. P3HT/bis-PCBM BHJ blend films were prepared according to the same spin-coating and annealing procedures. The weight ratio of the polymer/fullerene-derivatives of all the blend films prepared in the present study is 1 : 0.8. The mixtures of PCBM:bis-PCBM as the acceptor component with bis-PCBM compositions of 8 and 17 wt% were similarly prepared into P3HT/PCBM:8%-bisPCBM and P3HT/PCBM:17%bis-PCBM blend films. Pristine P3HT thin films were also similarly prepared as the reference for the thermal behavior of pure polymer crystallization. All films have a thickness of  $\sim 100 \text{ nm}$ . The corresponding BHJ solar cells based on the above films were fabricated with a device structure (ITO glass/PEDOT:PSS/BHJ active layer/Ca/Al). Basically, the GISAXS and GIWAXS intensities from the BHJ films (annealed at  $150^\circ\text{C}$  for 5–10 min) on the Si substrate and PEDOT:PSS layer, are almost the same. The effects of the PEDOT:PSS and Si substrates on the active layer and the scattering profiles are described in the ESI of our previous study.<sup>18</sup> The photocurrent-voltage curves of the corresponding cell devices and the preparation of the blend films were measured.<sup>44</sup>

Simultaneous GISAXS and GIWAXS measurements were conducted to investigate the pristine P3HT, P3HT/PCBM, P3HT/PCBM:8 and 17%bis-PCBM and P3HT/bis-PCBM blend films annealed at  $150^\circ\text{C}$  for  $t = 0$  (as-cast stage), 5, 120 and 360 min. The instrumental configuration and measurement procedure of the simultaneous GISAXS and GIWAXS experiments performed at the BL23A beam-line of the National Synchrotron Radiation Center (NSRRC) in Taiwan were described elsewhere.<sup>15</sup> All scattering data studying thermal stability were obtained in the same run/batch at the NSRRC. The GIWAXS profiles were reduced from the 2D GIWAXS patterns along the out-of-plane direction (perpendicular to the substrate and film surface, *i.e.*,  $z$  direction) and are expressed as a function of the scattering vector  $Q_z$ . The GISAXS profiles as a function of scattering vector  $Q_x$  were reduced from the 2D GISAXS patterns along the in-plane direction (parallel to the substrate, *i.e.*,  $x$  direction). The 2D GISAXS and 2D GIWAXS patterns were collected from different 2D detectors respectively. The GISAXS and GIWAXS detectors were located in different positions (scattering  $Q$  ranges) in the instrumental configuration.<sup>8</sup> The in-plane GISAXS

profiles are mainly used to determine the structures of the PCBM aggregated clusters and the large PCBM-rich domains. The 2D GISAXS pattern shows the anisotropic scattering, which is mainly comprised of in-plane  $Q_x$  and out-of-plane  $Q_z$  scattering (see Fig. 1e). This work mainly investigates the in-plane GISAXS profiles. The strong out-of-plane intensity is mainly from the main reflected beam rather than the scattering intensity contributed by PCBM clusters. Therefore, the out-of-plane GISAXS is not available to be analyzed herein. The out-of-plane GIWAXS profile reduced from the 2D GIWAXS pattern reveals the information of “edge-on” P3HT crystals. The out-of-plane GIWAXS profiles reveal the spacing between (100) layers, the size of the crystalline domain and the crystallinity of edge-on P3HT crystallites with lamellar structure (discussed later). The P3HT crystallites in the film mainly have two orientations: (1) the edge-on crystal with the lamellar (100) layer parallel to the film surface; (2) the face-on crystal with lamellar layer perpendicular to the film surface. Basically, the angular distribution of the orientation of the P3HT crystallites is anisotropic (see 2D GIWAXS pattern later). From the 2D WAXS pattern, the in-plane WAXS (along the in-plane direction) revealing the information of “face-on” P3HT crystals is too weak. The edge-on P3HT crystallite usually dominates in the films.

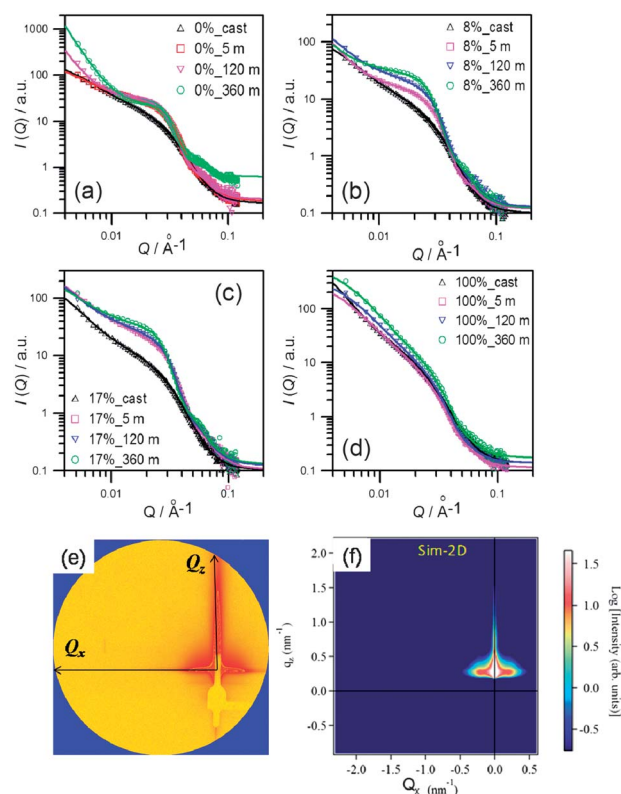


**Fig. 1** Time-dependent in-plane GISAXS profiles annealed at  $150^\circ\text{C}$  for (a) the P3HT/PCBM, (b) P3HT/PCBM:8%bis-PCBM, (c) P3HT/PCBM:17%bis-PCBM and (d) P3HT/bis-PCBM blend films. (Solid lines represent the GISAXS intensity calculated by the model fitting.) (e) Measured 2D GISAXS pattern of P3HT/PCBM blend film annealed at  $150^\circ\text{C}$  for 360 min. (The in-plane  $Q_x$  and out-of-plane  $Q_z$  directions are marked.) (f) Simulated 2D GISAXS pattern of the same film using the structure parameters obtained in Table 1 for comparison.

## Results and discussion

### Hierarchical phase separation of the P3HT/PCBM films from a BHJ structure to a thermally unstable structure

The in-plane GISAXS profiles of the P3HT/PCBM blend films annealed at 150 °C for  $t = 0$  (as-cast), 5 min (optimum BHJ stage), 120 min (early stage of thermal instability) and 360 min (thermally unstable stage) are shown in Fig. 1a. As our previous studies<sup>14,15</sup> and another report<sup>45</sup> pointed out, the main intensity in the medium- and high- $Q$  region (a broad peak at  $\sim 0.025 \text{ \AA}^{-1}$ ) of the GISAXS profiles is contributed by the spherical clusters aggregated by PCBM molecules and their interaction. The intensity upturn in the low- $Q$  region ( $0.005\text{--}0.1 \text{ \AA}^{-1}$ ) was attributed to the phase comprised of the amorphous P3HT polymer chains with the intercalated or dispersed PCBM molecules. This phase is called the PCBM/P3HT amorphous domain.<sup>18,46,47</sup> Compared to the low GISAXS intensity of the pure P3HT film (ESI, Fig. S1†), this upturn intensity is largely enhanced due to the increase of scattering contrast caused by the spatial distribution and number density of PCBM molecules dispersed or intercalated in the 3D network of the amorphous polymer chain. It reflects the characteristic length of the PCBM/P3HT amorphous domain. This upturn intensity can be modeled using the Debye–Anderson–Brumberger (DAB; also known as Debye–Bueche) equation with correlation length. This DAB model was frequently used in the model fitting of the GISAXS intensity for interpreting the large scale structure of the P3HT/PCBM systems in the other studies.<sup>14–16,45</sup> To simultaneously resolve the structures of the PCBM clusters and the PCBM/P3HT amorphous domains, the measured GISAXS profiles can be modeled as given by<sup>14</sup>

$$I(Q) = \frac{A}{[1 + (Q\xi)^2]^2} + \eta V(\Delta\rho)^2 \left[ \int_0^\infty F_i^2(Q, \sigma_i) f(\sigma_i) d\sigma_i + \int_0^\infty \int_0^\infty F_i(Q, \sigma_i) F_j(Q, \sigma_j) H_{ij}(Q, \sigma_i, \sigma_j) f_i(\sigma_i) f_j(\sigma_j) d\sigma_i d\sigma_j \right] \quad (1)$$

$$F_i(Q, \sigma_i) = 4\pi \left[ \sin(Q\sigma_i/2) - \frac{1}{2} Q\sigma_i \cos(Q\sigma_i/2) \right] \quad (2)$$

where the first term on the right-hand side is the DAB model,  $\xi$  is the correlation length of the PCBM-enriched/P3HT amorphous domain,  $A$  is a prefactor and is related to the product of the electron density contrast and  $\xi$ .<sup>3</sup> The second term on the right-hand side of eqn (1) is used to model the PCBM clusters assuming the polydispersed spheres have a Schultz size distribution with a hard-sphere interaction between the PCBM clusters.  $V$  is the average cluster volume.  $F(Q, \sigma_i)^2$  is the form factor of spherical PCBM clusters with a diameter  $\sigma_i$ .  $H(Q, \sigma_i, \sigma_j)$  is the pair structure function describing the interaction between clusters with the Percus–Yevick approximation (hard-sphere model). The analytical form was described elsewhere.<sup>48,49</sup> The fitting parameters,  $\eta$ ,  $R$  and  $p$  are the volume fraction, mean radius and polydispersity of size distribution of the PCBM clusters.  $\Delta\rho$  is the scattering contrast (difference of the scattering length densities between the cluster

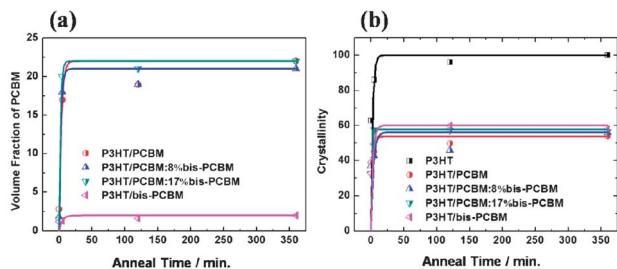
and matrix). All measured GISAXS profiles can be fitted well using the model of eqn (1).<sup>48</sup> The structural parameters,  $\xi$ ,  $A$ ,  $\eta$ ,  $R$  and  $p$ , obtained by the model fitting are listed in Table 1. Apparently, the significant increase of intensity in the medium- $Q$  region due to thermal annealing reveals the size growth and the increase in volume fraction of the PCBM clusters, enhancing the electron transport path in the BHJ structure. The fitted  $R$  values show the growth from 4.7 nm (as-casted) to 8.1 nm (annealed). The fitted volume fraction values of PCBM clusters also show a significant increase from 2.8 to 17%. Note that the volume fraction values,  $\eta$ , determined herein are only for a relative comparison rather than absolute values because the scattering contrast values estimated in the GISAXS experiment cannot be absolutely measured. Using the parameters obtained from the in-plane GISAXS analysis (shown in Table 1) for the P3HT/PCBM blend film annealed at 150 °C for 360 min as the grazing-incidence scattering geometry, we performed the simulation for a 2D GISAXS pattern, using the FitGISAXS simulation package. The simulated 2D GISAXS pattern agrees with the measured GISAXS pattern (Fig. 1). The agreement validates our in-plane GISAXS analysis and approach (see ESI for the details†).

The various characterization approaches and the associated structures of the morphology in the blend film are briefly introduced as follows. The mesoscale PCBM/P3HT amorphous domains and nanoscale PCBM clusters are determined by the in-plane GISAXS profiles fitted by the models of eqn (1). The orientation, crystal size, lamellar plane spacing and relative crystallinity of the nanoscale P3HT crystallites are determined by the reduced GIWAXS profiles (peak position and width) and 2D GIWAXS pattern. The macroscale PCBM segregation is observed by optical microscopy (discussed later). The PCBM- and P3HT-rich domains mediating between macro- and mesoscale length are investigated by various microscopies. Combined GISAXS and microscopy can interpret the nodular-like P3HT-rich domain (loose aggregation of nanoscale P3HT crystallites; discussed later).

For the P3HT/PCBM blend films, the variation of the broad peaks of the GISAXS profiles (in the medium- $Q$  region of Fig. 1a) with annealing times from 5 to 360 min remains stable, suggesting that the nanoscale PCBM clusters almost do not change in the course of annealing. Note that the intensity upturn in the low- $Q$  region of the GISAXS profile for the film annealed for 5 min is identical to that of the as-cast film. This inert behavior of intensity upturn in the initial period is consistent with the previous independent GISAXS result (at 150 °C for 0–30 min).<sup>15</sup> According to the GISAXS analysis (Table 1) under the condition of long-term annealing, there are two significant findings beyond our current knowledge on the thermal instability: (1) the nanoscale PCBM clusters (16–18 nm; Table 1) do not vary with the annealing time from the optimum BHJ structure (5 min) to the thermally unstable stage (360 min). The temporal behavior (Fig. 2a) of cluster volume fraction in the initial period (forming the optimum BHJ structure) is consistent with that reported in the literature<sup>15</sup> (using the well-known Avrami equation). The initial kinetics are fast. Then, the nanoscale PCBM clusters attain saturation (stable) behavior of size and volume fraction, although the phase separation regime transits to the thermally

**Table 1** Structural parameters obtained by SAXS model fitting analysis for P3HT/fullerene-derivative films annealed at 150 °C for various times together with corresponding PCE values

Acceptor	<i>t</i> (min)	$\eta$ (%)	<i>R</i> (nm)	<i>p</i>	<i>A</i>	$\xi$ (nm)	PCE (%)
PCBM	0	2.8	4.7	0.46	$4.23 \times 10^{-5}$	17.3	n/a
	5	17	8.1	0.28	$3.26 \times 10^{-5}$	18.0	3.00
	120	19	8.7	0.28	$6.95 \times 10^{-5}$	70.0	2.55
	360	22	9.0	0.23	$89.5 \times 10^{-5}$	301.5	1.74
PCBM:8%bis-PCBM	0	1.8	4.4	0.47	$2.16 \times 10^{-5}$	19.0	n/a
	5	18	8.2	0.32	$1.50 \times 10^{-5}$	36.4	3.62
	120	19	8.5	0.34	$1.90 \times 10^{-5}$	27.9	3.56
	360	21	9.7	0.29	$1.09 \times 10^{-5}$	35.0	3.61
PCBM:17%bis-PCBM	0	1.4	4.2	0.49	$2.37 \times 10^{-5}$	22.8	n/a
	5	20	8.0	0.37	$3.46 \times 10^{-5}$	22.9	3.36
	120	21	8.7	0.35	$2.96 \times 10^{-5}$	24.6	3.40
	360	22	9.8	0.31	$2.90 \times 10^{-5}$	21.5	3.45
Bis-PCBM	0	1.2	3.8	0.64	$5.89 \times 10^{-5}$	31.2	n/a
	5	1.3	6.3	0.38	$6.95 \times 10^{-5}$	17.7	2.98
	120	1.6	7.4	0.28	$11.0 \times 10^{-5}$	15.6	3.04
	360	2.0	7.6	0.24	$18.4 \times 10^{-5}$	15.7	3.15

**Fig. 2** Kinetic behaviors of (a) the volume fraction of PCBM clusters and (b) the P3HT crystallization. Their fitting curves demonstrate that the saturation behavior is quickly attained.

unstable stage. (2) The size of the PCBM/P3HT amorphous domain (approximated by correlation length) remarkably increases with the annealing time from 18.0 nm for  $t = 5$  min to 301.5 nm for  $t = 360$  min, as evidenced by the sharp increase in the slope of the intensity upturn in the low- $Q$  region (Fig. 1a). Moreover, the concurrent dramatic increase in the prefactor  $A$  signifies that the number density of PCBM molecules in the amorphous domain increases during thermal aging. In contrast, the GISAXS intensities in the same low- $Q$  region of the pure P3HT polymers annealed for different times still do not vary and are much weaker (see ESI, Fig. S1†), implying the weak electron scattering contrast for the pure polymer domain. This difference between the GISAXS profiles of the annealed P3HT and P3HT/PCBM films shows that the increase of the low- $Q$  intensity is closely related to the increase in the number of PCBM molecules within the amorphous polymer domains. The enhanced contrast due to the thermal annealing helps the detection of the domain size. This structural evolution (growth) of this PCBM/P3HT amorphous domain on the scale of 20–300 nm is defined as the mesoscale here (Table 1) and can be quantitatively characterized. In contrast, the related TEM images of the mesoscale structures show P3HT-rich and PCBM-rich domains, which are scarcely distinctive (ESI, Fig. S3†).

The remarkable growth and PCBM-richness of these amorphous domains during the thermally unstable stage can be considered as an independent mesoscale phase separation process, which is revealed for the first time. It causes the large scale formation of PCBM-depleted or almost pure polymer domains. The evolution of these mesoscale domains is closely related to the concurrent occurrence of micro-sized PCBM-rich segregation (defined as the macroscale here). Previous literature<sup>50</sup> has demonstrated that P3HT and PCBM form a charge-transfer complex in the solid blend through donating partial charge on the sulfur atom of thiophene ring to the  $C_{60}$  cage that lightly binds PCBM molecules among 3HT units in the amorphous P3HT domains. Based on this point, our speculation on the mechanism is that upon heating the blend beyond the glass transition temperature of P3HT, the thermal motion of polymer chains can induce the close contact of these P3HT-binded PCBM molecules, and then the strong  $\pi$ - $\pi$  interaction of the  $C_{60}$  units may glue them together to generate mesoscale amorphous PCBM-rich domains. They may further coalesce or develop into macroscale domains/or clusters during the long-term annealing at high temperature. The dramatic degradation of the PCE values corresponding to each stage from BHJ to a thermally unstable structure is shown in Table 1. The corresponding optical microscopy (OM) observation for the growth of macroscale domains in the P3HT/PCBM films prepared with the same procedure consistently shows the temporal behavior, which is shown elsewhere.<sup>44</sup> Similar OM images for the temporal behavior of the macroscale segregation are also reported by several studies.

In short conclusion, the size of the PCBM clusters (scale of 10–20 nm; defined as the nanoscale here) is stable from the formation of the optimum BHJ structure to the thermally unstable stage. The mesoscale PCBM/P3HT amorphous domains ( $\sim 100$  nm on average) remain identical for both the as-cast and optimum BHJ films. Both the amorphous domains seem not to contribute to the enhanced performance due to the

annealing. However, the amorphous domains become more PCBM-rich blends and the domain sizes steadily grow, starting from the early stage of instability ( $t = 120$  min). The growth of the mesoscale domains play an important role in the degradation of performance in the thermally unstable stage (as indicated by the corresponding PCE values in Table 1). It can be considered as a type of loose aggregation that reduces the interface area between P3HT and PCBM on the molecular scale. Both the mesoscale PCBM/P3HT amorphous domains and the macroscale PCBM-rich domains would concurrently reduce the total interfacial area. The present GISAXS analysis also shows that the nanoscale PCBM clusters do not develop (or coalesce) into the mesoscale PCBM clusters (ESI, Fig. S2†). The time-dependent GISAXS profiles clearly show the evolutions corresponding to the nanoscale and mesoscale structures are independent. This model-dependent analysis is self-consistent with the interpretation of the other experimental results discussed later. Put simply, the behavior of the phase separation has two independent regimes at the nano and meso scales, respectively, during the BHJ-forming stage and the thermally unstable stage. Two different mechanisms for nano and meso scale phase separation are proposed to explain the observed phenomena. The nanoscale PCBM clusters are confined by the surrounding nanoscale P3HT crystallites so that they cannot move and further coalesce. Because they do not dissolve, the source of the PCBM molecules for developing the amorphous domains is another source with a fixed amount in the mesoscale phase. A mistaken impression in the past is that the nanoscale PCBM cluster is closely related to the large scale of PCBM segregation and thermal degradation. Our new information clarifies that the real target of suppressing the thermal instability and the degraded performance is to inhibit or control the growth of the mesoscale amorphous P3HT/PCBM domain rather than the nanoscale PCBM cluster.

Fig. 3a and b show the out-of-plane GIWAXS profiles of the annealed pristine P3HT and P3HT/PCBM blend films corresponding to the simultaneous GISAXS measurements. The lamellar spacing of (100) layers ( $= 2\pi/Q$ ), crystal size and relative crystallinity of the edge-on P3HT crystalline domains can be determined by the peak position, full-width at half-maximum (FWHM) and normalized integrated area of the (100) peak.<sup>14,15,18,51</sup> The results are summarized in Table 2. The literature<sup>15,52</sup> pointed out that the crystallization of the P3HT polymer is mutually confined by the PCBM aggregation into clusters. The kinetic behaviors of both the PCBM and P3HT components (Fig. 2) were similar during the BHJ-forming stage. Moreover, the crystallinity of the nanoscale P3HT crystal remains stable from the BHJ structure to the thermally unstable structure. Additionally, the growth behavior of the P3HT crystal size (10–16 nm) during all the stages is also affected by the mutual confinement effect from the PCBM clusters (Table 2). On the other hand, the development (extension due to ordering of the side chain) of lamellar spacing in the pristine P3HT and P3HT/PCBM crystals during the BHJ-forming stage (Table 2) is consistent with that previously reported.<sup>14,15,18</sup> Notably, for the P3HT/PCBM blend film, a special phenomenon that the lamellar spacing abnormally shrinks from 16.43 to 15.97 Å, is observed at the thermally unstable stage

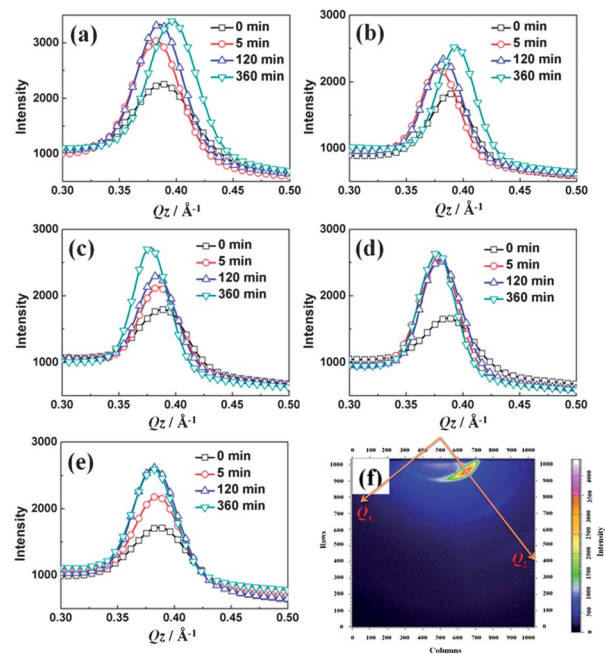


**Fig. 3** Temporal variation of the out-of-plane GIWAXS profiles for (a) the pristine P3HT film, (b) P3HT/PCBM, (c) P3HT/PCBM:8%bis-PCBM (d) P3HT/PCBM:17%bis-PCBM and (e) P3HT/bis-PCBM blend films annealed at 150 °C. (f) 2D GIWAXS pattern of P3HT/bis-PCBM blend film annealed at 150 °C for 360 min. (The in-plane  $Q_x$  and out-of-plane  $Q_z$  directions are marked).

(*i.e.*,  $t = 360$  min), as evidenced by the remarkable shift of the (100) peak (Fig. 3b). A similar behavior (from 16.32 to 15.86 Å) is also found for the pure P3HT polymer. It reveals that this shrinkage is attributed to the thermal contraction (or disorder) of side chains (along the [100] direction) of the pure polymer at the thermally unstable stage. Note that the fibril-like or nodular-like

**Table 2** The relative crystallinity, crystal size ( $L$ ) and lamellar spacing ( $d$ ) determined by GIWAXS profiles corresponding to the SAXS analysis of Table 1

Film	$t$ (min)	$d$ (Å)	$L$ (Å)	Rel. crystallinity (%)
P3HT	0	16.14	96.25	62.74
	5	16.43	123.20	86.22
	120	16.32	131.06	96.15
	360	15.86	128.33	100
P3HT/PCBM	0	16.14	136.89	38.82
	5	16.61	154.00	45.15
	120	16.43	157.95	49.77
P3HT/PCBM:8%bis-PCBM	0	16.10	108.07	36.88
	5	16.39	143.26	42.63
	120	16.39	157.95	45.96
P3HT/PCBM:17%bis-PCBM	0	16.32	106.21	32.57
	5	16.61	154.00	57.62
	120	16.55	160.00	57.36
P3HT/bis-PCBM	0	16.32	102.67	32.75
	5	16.32	131.06	49.43
	120	16.43	140.00	60.05
	360	16.43	150.24	58.10

P3HT crystals with macroscale or mesoscale lengths reported by the general microscopic observations can be regarded as a loose aggregation of nanoscale P3HT crystals with non-contact form. The mesoscale aggregation of nano P3HT crystals is also consistent with the previous GISAXS study for the pure polymer. Because its scattering contrast and contribution to GISAXS are very weak, we ignore this structure here compared to the PCBM cluster.

### Phase separation of P3HT/PCBM:*x*%bis-PCBM film with tunable and thermally stable mesoscale domain

In the previous study,<sup>44</sup> a few bis-PCBM molecules ( $\geq 8$  wt%) incorporated into the PCBM acceptor molecules can effectively suppress the macroscale PCBM-rich segregation. However, the mechanism is still unknown, providing the motivation for the present study. After understanding the evolution of the hierarchical structure of each component in the P3HT/PCBM film from the BHJ structure to the thermally unstable structure, there is an interesting issue: how do the bis-PCBM molecules as a part of the acceptor component influence the aggregation of PCBM molecules into clusters, the growth of the PCBM/P3HT amorphous domain and the self-organization (crystallization) of the P3HT on the nanoscale and mesoscale? The knowledge solving this question can be extended to fundamentally understand the universal mechanism of the various approaches used to inhibit the phase segregation of thermal instability. In this section, we further examine if the mesoscale domain plays a key role in the universal mechanism. The simultaneous in-plane GISAXS and out-of-plane GIWAXS profiles measured for the P3HT/PCBM:8% bis-PCBM blend films annealed at 150 °C for  $t = 0$ –360 min are shown in Fig. 1b and 3c, respectively. The GISAXS and GIWAXS profiles of the P3HT/PCBM:17%bis-PCBM blend films processed with the same procedure are shown in Fig. 1c and 3d. The GISAXS and GIWAXS profiles of the P3HT/PCBM:8%bis-PCBM blend films annealed to give various structural stages are similar to those of the P3HT/PCBM:17%bis-PCBM blend films, revealing similar hierarchical structures and bis-PCBM-content-independent behavior. Their GISAXS profiles can be fitted well using the model of eqn (1). The structural parameters determined by model fitting are listed in Table 1. The TEM images of the P3HT/PCBM:8%bis-PCBM film annealed at 150 °C for 10, 120 and 360 min show the nanoscale fullerene clusters (dark dots marked) with a size close to that revealed by our GISAXS study (ESI, Fig. S3†). The corresponding PCE values from the BHJ structure to the thermally unstable structure remain stable (Table 1), showing the distinctive thermal stability compared to the conventional polymer solar cell. The corresponding OM observations for the similarly prepared P3HT/PCBM films consistently show almost no macroscale segregation.<sup>44</sup>

The time-dependent GISAXS profiles of the P3HT/PCBM:8% bis-PCBM blend films are different from those of the P3HT/PCBM blend films. According to the model-fitting result (Table 1), the volume fraction  $\eta$  and radius  $R$  of the nanoscale fullerene clusters in the BHJ and thermally unstable structures for the P3HT/PCBM films are close to those obtained for the P3HT/PCBM:8%bis-PCBM blend films. Also, the kinetic behavior of

fullerene clustering is the same for both sets of films (Fig. 2a). The effect of bis-PCBM incorporation has no influence on the formation of nanoscale PCBM clusters. As we mentioned, the nanoscale and mesoscale phase separations are independent of each other. Notably, the size and PCBM-content of the mesoscale PCBM/P3HT amorphous domains in the BHJ structure of the P3HT/PCBM:8%bis-PCBM blend films are much smaller than those of the P3HT/PCBM films (Table 1). Moreover, the growth and PCBM-densification of the mesoscale PCBM/P3HT amorphous domains are effectively inhibited during the phase transformation from the BHJ to unstable structure stage. The structural evolution and high thermal stability are consistent with those of the inhibited macroscale PCBM-rich domains, whose corresponding OM observation is shown in the previous study.<sup>44</sup> The present work justifies again that the macroscale segregation concurrently develops with the mesoscale PCBM-rich domains. The suppression of the mesoscale domain, as directly evidenced by our GISAXS profiles of the P3HT/PCBM:8%bis-PCBM blend film, leads to the large reduction in the macroscale domain. The thermal instability is mainly governed by the development and thermal behavior of mesoscale domains, which is demonstrated for the first time in the present study. Therefore, the structure and good thermal stability of the mesoscale PCBM/P3HT amorphous domain tuned by the bis-PCBM molecules as an example of control factor is critical from the phenomenological viewpoint. The data in the next subsection provides more mechanistic discussion.

The growth kinetics of nanoscale P3HT crystals in the P3HT/PCBM:8%bis-PCBM blend films have a similar trend with nanoscale PCBM clustering during all stages (Fig. 2). However, for the as-cast films, the incorporation of a few bis-PCBM molecules would lead to a decrease in the crystal size (Table 2) compared to the P3HT/PCBM film. It reveals that the bis-PCBM molecules can affect the crystallization behavior during the solution-drying process. Interestingly, the evolution of the lamellar spacing in the thermally unstable stage ( $t = 360$  min) of the P3HT/PCBM:8%bis-PCBM blend film is different from that of the P3HT/PCBM blend film (indicated by the shift of peak position in Fig. 3b and c). The shrinkage of lamellar spacing disappears due to the presence of bis-PCBM molecules. This finding can be explained as the bis-PCBM molecules cause the spatially dense distribution of fullerene molecules intercalated around the boundary of the crystalline domain (and partly located between the rims of the (100) layer) so that the contraction of the polymer side chain along the [100] direction is suppressed.<sup>10</sup> These phenomena can be partly understood by the fact that bis-PCBM has a higher solubility than that of PCBM so the former can form a more homogeneous blend with P3HT than the latter does during the solution-drying process, leading to a lower crystallinity and a smaller crystallite size of P3HT in the as-cast P3HT/bis-PCBM film, and a higher bis-PCBM concentration in the mesoscale P3HT amorphous domains.

### Phase separation of P3HT/bis-PCBM film

To further explore the mechanism, we need to understand how various interactions between different molecules and molecular

motions proceed. These questions have never been analytically discussed. For example, what is the role of the bis-PCBM molecules participating in the nanoscale fullerene-clustering process in the solution-drying or annealing process? How does the bis-PCBM inhibit the formation of macroscale and mesoscale segregations? Therefore, simultaneous GISAXS and GIWAXS measurement was conducted for the P3HT/bis-PCBM films similarly prepared. The discrepancy in the characteristics of the GISAXS profiles of this systematic study can provide enough information for resolving the above questions. Interestingly, the time-dependent GISAXS profiles of the P3HT/bis-PCBM films demonstrate totally different shape, structural evolution behavior and model-fitting results (Fig. 1d) and (Table 1). The volume fraction  $\eta$  and radius  $R$  of the nanoscale bis-PCBM clusters are 2% and 7.6 nm, respectively, which are much smaller than those of the other films (*cf.* 22% and 9.0 nm for PCBM clusters under the same conditions). This finding indicates that the two substituents on each C<sub>60</sub> core substantially obstruct the self-aggregation of bis-PCBM molecules into large clusters through the  $\pi$ - $\pi$  interaction of neighboring fullerene cages. Similarly, the additional substituent in bis-PCBM will lower its ability to form a charge-transfer complex with P3HT during the thermal motion of the polymer. This speculation can explain why the mesoscale bis-PCBM/P3HT amorphous domain in the P3HT/bis-PCBM film is relatively small and thermally stable. On the other hand, because the bis-PCBM molecules form much fewer nanoscale clusters, the number of the bis-PCBM molecules left outside the bis-PCBM/P3HT amorphous domain would be much higher. These amorphous-nature bis-PCBM molecules in the matrix further reinforce the blocking effect to cause the small amorphous domain. The nanoscale bis-PCBM clusters are small and few so that the charge transport effect is reduced and thus the PCE values (short-circuit currents) in the P3HT/bis-PCBM device are much lower than in the other films (Table 1). This result can also explain the thermal stability of the P3HT/PCBM:*x*%bis-PCBM blend film. Because of the low ability of the bis-PCBM forming the charge-transfer complex with P3HT shown herein, the P3HT-binded PCBM molecules are covered with or screened by bis-PCBM, although the fraction of bis-PCBM is small. The ability of intermolecular PCBM aggregation, or formation of more P3HT-binded PCBM complex (under the thermal motion of polymer in the domains), would be reduced due to the presence of the bis-PCBM. It consequently suppresses the thermal growth (and PCBM-richness) of the amorphous mesoscale domains. The details of the interaction model cannot be solved in the present study and would be a working target in the future.

The nanoscale fullerene cluster tends to be formed purely by the PCBM molecules, while almost all the bis-PCBM molecules stay in (1) the mesoscale PCBM/P3HT amorphous polymer domains and (2) the zones outside the domains and P3HT crystals. The data showing that the volume fraction and radius of the nanoscale clusters in the P3HT/PCBM:*x*%bis-PCBM films remain the same as those of the P3HT/PCBM films (Table 1) support this finding. Thus, the good electron transport path, mainly contributed by the size and volume fraction of the PCBM clusters, remains. The significant suppression of the thermal growth of

the mesoscale fullerene-rich amorphous polymer domain is caused by the hindering effect of bis-PCBM molecules on the molecular interaction between the amorphous polymer chain (with the thermal motion) and PCBM molecules. According to the variation of lamellar spacing determined by the shift of the peak positions of GIWAXS profiles, several bis-PCBM molecules also prefer to partly locate between the rims of the (100) layer of the P3HT crystalline domain and freeze the lamellar structure of the crystal during the thermally unstable stage.

These points provide new understanding and insight into the mechanism of control strategies (2), (3) and (6) (mentioned in the Introduction section) for suppressing the macroscale phase segregation. Using high  $T_g$  polymers or constructing distinctive polymer networks to confine the thermal motion of the polymer chains are effective approaches to lower the segregation of PCBM-rich amorphous domains into macroscale clusters. However, the thermally stiff main chains and the disturbance of the crosslinking bridges may decrease the crystallinity of conjugated backbones, thereby lowering the carrier mobility. By tuning the solubility and substituent characteristics of two fullerene derivatives, the main PCBM molecules can independently form the optimum nanoscale charge transport path, which is not influenced by the other fullerene derivative as inhibitor. The critical route proposed here is to directly control the size and thermal stability of the mesoscale fullerene-rich amorphous domain. The rational strategy that not only keeps the optimum BHJ structure (nanoscale charge transport path and interface area between donor and acceptor) in the initial annealing but also controls the thermal instability (mainly related to the mesoscale fullerene/polymer domain) is feasible. The morphological control and thermal evolution of the nanoscale structure is independent of those of the mesoscale structure. These findings are revealed for the first time. Therefore, we suggest that one can still use or design a mixture of conducting polymer and PCBM with the desired content for the initial optimum BHJ structure with high efficiency. Then one can select a form of aggregation inhibitor (like the bis-PCBM used here or the other modified polymer) at low concentration. The mutual influence among the specially selected molecules, PCBM molecules and the designed polymer would play an important role in controlling the mesoscale fullerene/polymer amorphous domain, which is the origin of the macroscale segregation. This approach will make the fabrication of low cost, high performance and high thermal stability of a BHJ polymer solar cell possible. For P3HT/fullerene solar cells, the normal performance is contributed by the nanoscale as well as mesoscale structures for charge separation and transport. For some low band-gap polymer solar cells with high performance, the nanoscale PCBM structures aggregate into mesoscale domains of several hundred nanometers (tailored by additives), demonstrating the different role of mesoscale PCBM/polymer structures. It is under-investigated.

## Conclusions

The structural evolutions on the multi-length scales from the formation of a BHJ structure stage to a thermally unstable



hierarchical structure stage have been studied by a simultaneous GISAXS and GIWAXS technique. The results indicate that phase separation regimes on the nano- and meso-scale in the BHJ and thermally unstable structures are independent of each other. The kinetic behavior of the nanoscale PCBM clusters and P3HT crystals is very stable during long-term annealing at 150 °C, while the mesoscale PCBM-rich/P3HT amorphous domain grows remarkably with annealing time from the BHJ stage to the unstable structure stage. The macroscale PCBM-rich segregation is developed concurrently with the mesoscale domain, which can be considered as the local coalescence of heterogeneous mesoscale domains during the course of long-term annealing. Controlling the structural evolution and thermal stability of the mesoscale domains during heating would be a critical factor for suppressing the thermal instability rather than those of the nanoscale BHJ structure. It can be concluded that the morphological control and thermal evolution of nanoscale structures (optimum BHJ structure) is independent of those of mesoscale structures (origin of thermally unstable macrostructure or macroscale segregation). The mutual influence on the PCBM of the fullerene derivative as an inhibitor (for example, bis-PCBM) and the polymer during the hierarchical structural evolution in the systematic study proposes the mechanisms of thermal instability and effective control strategy for a polymer/fullerene-based solar cell. The present study significantly advances the general knowledge of the thermal instability arising from the nanoscale BHJ structure. This knowledge could aid in the design of thermally stable polymers and high performance solar cells with low-cost, good stability and easy-fabrication advantages.

## Acknowledgements

We thank financial support obtained from National Science Council (99-2113-M-002-001-MY3, 100-2120-M-002-007 and 100-3113-E-002-012) and Institute of Nuclear Energy Research (National Project of Energy; 10120011NER030), Taiwan.

## Notes and references

- 1 S. S. V. Bavel, E. Sourty, G. D. With and J. Loos, *Nano Lett.*, 2009, **9**, 853–855.
- 2 W. Ma, C. Yang, X. Gong, K. Lee and A. J. Heeger, *Adv. Funct. Mater.*, 2005, **15**, 1617–1622.
- 3 Y. Sun, C. Cui, H. Wang and Y. Li, *Adv. Energy Mater.*, 2012, **2**, 966–969.
- 4 J. S. Kim, W. S. Chung, K. Kim, D. Y. Kim, K. J. Paeng, S. M. Jo and S. Y. Jang, *Adv. Funct. Mater.*, 2010, **20**, 3538–3546.
- 5 M. Jørgensen, K. Norrman and F. C. Krebs, *Sol. Energy Mater. Sol. Cells*, 2008, **92**, 686–714.
- 6 R. A. Marsh, J. M. Hodgkiss, S. Albert-Seifried and R. H. Friend, *Nano Lett.*, 2010, **10**, 923–930.
- 7 G. Li, V. Shrotriya, J. Huang, Y. Yao, T. Moriarty, K. Emery and Y. Yang, *Nat. Mater.*, 2005, **15**, 1617–1622.
- 8 J. Peet, J. Y. Kim, N. E. Coates, W. L. Ma, D. Moses, A. J. Heeger and G. C. Bazan, *Nat. Mater.*, 2007, **6**, 497–500.
- 9 Y.-M. Chang and L. Wang, *J. Phys. Chem. C*, 2008, **112**, 17716–17720.
- 10 B. A. Collins, Z. Li, J. R. Tumbleston, E. Gann, C. R. McNeill and H. Ade, *Adv. Energy Mater.*, 2013, **3**, 65–74.
- 11 M. R. Hammond, R. J. Kline, A. A. Herzog, L. J. Richter, D. S. Germack, H.-W. Ro, C. L. Soles, D. A. Fischer, T. Xu, L. Yu, M. F. Toney and D. M. DeLongchamp, *ACS Nano*, 2011, **5**, 8248–8257.
- 12 C. V. Hoven, X.-D. Dang, R. C. Coffin, J. Peet, T.-Q. Nguyen and G. C. Bazan, *Adv. Mater.*, 2010, **22**, E63–E66.
- 13 S. J. Lou, J. M. Szarko, T. Xu, L. Yu, T. J. Marks and L. X. Chen, *J. Am. Chem. Soc.*, 2011, **133**, 20661–20663.
- 14 H. C. Liao, C. S. Tsao, T. H. Lin, C. M. Chuang, C. Y. Chen, U. S. Jeng, C. H. Su, Y. F. Chen and W. F. Su, *J. Am. Chem. Soc.*, 2011, **133**, 13064–13073.
- 15 W. R. Wu, U. S. Jeng, C. J. Su, K. H. Wei, M. S. Su, M. Y. Chiu, C. Y. Chen, W. B. Su, C. H. Su and A. C. Su, *ACS Nano*, 2011, **5**, 6233–6243.
- 16 B. A. Collins, J. R. Tumbleston and H. Ade, *J. Phys. Chem. Lett.*, 2011, **2**, 3135–3145.
- 17 R. Giridharagopal and D. S. Ginger, *J. Phys. Chem. Lett.*, 2010, **1**, 1160–1169.
- 18 Y. C. Huang, C. S. Tsao, C. M. Chuang, C. H. Lee, F. H. Hsu, H. C. Cha, C. Y. Chen, T. H. Lin, C. J. Su, U. S. Jeng and W. F. Su, *J. Phys. Chem. C*, 2012, **116**, 10238–10244.
- 19 S. J. Lou, J. M. Szarko, T. Xu, L. Yu, T. J. Marks and L. X. Chen, *J. Am. Chem. Soc.*, 2011, **133**, 20661–20663.
- 20 W. Chen, T. Xu, F. He, W. Wang, C. Wang, J. Strzalka, Y. Liu, J. Wen, D. J. Miller, J. Chen, K. Hong, L. Yu and S. B. Darling, *Nano Lett.*, 2011, **11**, 3707–3713.
- 21 F. He, W. Wang, W. Chen, T. Xu, S. B. Darling, J. Strzalka, Y. Liu and L. Yu, *J. Am. Chem. Soc.*, 2011, **133**, 3284–3287.
- 22 H. C. Liao, C. S. Tsao, T. H. Lin, M. H. Jao, C. M. Chuang, S. Y. Chang, Y. C. Huang, Y. T. Shao, C. Y. Chen, C. J. Su, U. S. Jeng, Y. F. Chen and W. F. Su, *ACS Nano*, 2012, **6**, 1657–1666.
- 23 Y. Gu, C. Wang and T. P. Russell, *Adv. Energy Mater.*, 2012, **2**, 683–690.
- 24 W. Chen, M. P. Nikiforov and S. B. Darling, *Energy Environ. Sci.*, 2012, **5**, 8045–8074.
- 25 J. Rivnay, S. C. B. Mannsfeld, C. E. Miller, A. Salleo and M. F. Toney, *Chem. Rev.*, 2012, **112**, 5488–5519.
- 26 Y. M. Chang, W. F. Su and L. Wang, *Sol. Energy Mater. Sol. Cells*, 2008, **92**, 761–765.
- 27 N. Grossiord, J. M. Kroon, R. Andriessen and P. W. M. Blom, *Org. Electron.*, 2012, **13**, 432–456.
- 28 C. J. Brabec, S. Gowrisanker, J. J. M. Halls, D. Laird, S. Jia and S. P. Williams, *Adv. Mater.*, 2010, **22**, 3839–3856.
- 29 C. H. Woo, B. C. Thompson, B. J. Kim, M. F. Toney and J. M. J. Fréchet, *J. Am. Chem. Soc.*, 2008, **130**, 16324–16329.
- 30 K. Sivula, C. K. Luscombe, B. C. Thompson and J. M. J. Fréchet, *J. Am. Chem. Soc.*, 2006, **128**, 13988–13989.
- 31 Z. Zhou, X. Chen and S. Holdcroft, *J. Am. Chem. Soc.*, 2008, **130**, 11711–11718.
- 32 S. Bertho, G. Janssen, T. J. Cleij, B. Conings, W. Moons, A. Gadisa, J. D'Haen, E. Goovaerts, L. Lutsen, J. Manca and

- D. J. M. Vanderzande, *Sol. Energy Mater. Sol. Cells*, 2008, **92**, 753–760.
- 33 S. Bertho, I. Haeldermans, A. Swinnen, W. Moons, T. Martens, L. Lutsen, D. J. M. Vanderzande, J. Manca, A. Senes and A. Bonfiglio, *Sol. Energy Mater. Sol. Cells*, 2007, **91**, 385–389.
- 34 J. Vandenberg, B. Conings, S. Bertho, J. Kesters, D. Spoltore, S. Esiner, J. Zhao, G. V. Assche, M. M. Wienk, W. Maes, L. Lutsen, B. V. Mele, R. A. J. Janssen, J. Manca and D. J. M. Vanderzande, *Macromolecules*, 2011, **44**, 8470–8478.
- 35 S. Miyanishi, K. Tajima and K. Hashimoto, *Macromolecules*, 2009, **42**, 1610–1618.
- 36 B. J. Kim, Y. Miyamoto, B. Ma and J. M. J. Fréchet, *Adv. Funct. Mater.*, 2009, **19**, 2273–2281.
- 37 J. U. Lee, J. W. Jung, T. Emrick, T. P. Russell and W. H. Jo, *J. Mater. Chem.*, 2010, **20**, 3287–3294.
- 38 J. B. Kim, K. Allen, S. J. Oh, S. Lee, M. F. Toney, Y. S. Kim, C. R. Kagan, C. Nuckolls and Y. L. Loo, *Chem. Mater.*, 2010, **22**, 5762–5773.
- 39 Y. C. Lai, T. Higashihara, J. C. Hsu, M. Ueda and W. C. Chen, *Sol. Energy Mater. Sol. Cells*, 2012, **97**, 164–170.
- 40 J. H. Tsai, C. C. Chueh, M. H. Lai, C. F. Wang, W. C. Chen, B. T. Ko and C. Ting, *Macromolecules*, 2009, **42**, 1897–1905.
- 41 J. H. Tsai, Y. C. Lai, T. Higashihara, C. J. Lin, M. Ueda and W. C. Chen, *Macromolecules*, 2010, **43**, 6085–6091.
- 42 S. O. Kim, D. S. Chung, H. Cha, J. W. Jang, Y. H. Kim, J. W. Kang, Y. S. Jeong, C. E. Park and S. K. Kwon, *Sol. Energy Mater. Sol. Cells*, 2011, **95**, 432–439.
- 43 Y. Zhang, H. L. Yip, O. Acton, S. K. Hau, F. Huang and A. K. Y. Jen, *Chem. Mater.*, 2009, **21**, 2598–2600.
- 44 H. W. Liu, D. Y. Chang, W. Y. Chiu, S. P. Rwei and L. Wang, *J. Mater. Chem.*, 2012, **22**, 15586–15591.
- 45 W. Kiel, A. P. R. Eberle and M. E. Mackay, *Phys. Rev. Lett.*, 2010, **105**, 168701.
- 46 A. Zen, M. Saphiannikova, N. Dieter, J. Grenzer, S. Grigorian, U. Pietsch, U. Asawapirom, S. Janietz, U. Scherf, I. Lieberwirth and G. Wegner, *Macromolecules*, 2006, **39**, 2162–2171.
- 47 N. D. Treat, M. A. Brady, G. Smith, M. F. Toney, E. J. Kramer, C. J. Hawker and M. L. Chabinyc, *Adv. Energy Mater.*, 2011, **1**, 82–89.
- 48 S. R. Kline, *J. Appl. Crystallogr.*, 2006, **39**, 895–900.
- 49 W. L. Griffith, R. Triolo and A. L. Compere, *Phys. Rev. A: At., Mol., Opt. Phys.*, 1987, **35**, 2200–2206.
- 50 V. Shrotriya, J. Ouyang, R. J. Tseng, G. Li and Y. Yang, *Chem. Phys. Lett.*, 2005, **411**, 138–143.
- 51 E. Verploegen, R. Mondal, C. J. Bettinger, S. Sok, M. F. Toney and Z. Bao, *Adv. Funct. Mater.*, 2010, **20**, 3519–3529.
- 52 J. Jo, S. S. Kim, S. I. Na, B. K. Yu and D. Y. Kim, *Adv. Funct. Mater.*, 2009, **19**, 866–874.